Inductance Formula for Rectangular Planar Spiral Inductors with Rectangular Conductor Cross Section

H. A. Aebischer[1]*

[1]LEGIC Identsystems AG, Switzerland
*corresponding author, E-mail: hubert.aebischer@legic.com

Abstract

In modern technology, inductors are often shaped in the form of planar spiral coils, as in radio frequency integrated circuits (RFIC's), 13.56 MHz radio frequency identification (RFID), near field communication (NFC), telemetry, wireless charging, and eddy current nondestructive testing devices, where the coils must be designed to a specified inductance. In many cases, the direct current (DC) inductance is a good approximation. Some approximate formulae for the DC inductance of planar spiral coils with rectangular conductor cross section are known from the literature. They can simplify coil design considerably. But they are almost exclusively limited to square coils.

This paper derives a formula for rectangular planar spiral coils with an aspect ratio of up to 4.0 and having a cross-sectional aspect ratio of height to width not exceeding unity. It is based on physical principles, hence scalable and valid for any dimension and inductance range.

The formula lowers the overall maximum error from hitherto 28 % down to 5.6 %. For specific application areas like RFIC's and RFID antennas, it is possible to reduce the domain of definition, with the result that the formula lowers the maximum error from so far 18 % down to 2.6 %. This was tested systematically on close to 194000 coil designs of exactly known inductance. To reduce the number of dimensions of the parameter space, dimensionless parameters are introduced. The formula was also tested against measurements taken on 16 RFID antennas manufactured as printed circuit boards (PCB's).

The derivation is based on the idea of treating the conductor segments of all turns as if they were parallel conductors of a single-turn coil. It allows the inductance to be calculated with the help of mean distances between two arbitrary points anywhere within the total cross section of the coil. This leads to compound mean distances that are composed of two types of elementary ones, firstly, between a single rectangle and itself, and secondly, between two displaced congruent rectangles. For these elementary mean distances, exact expressions are derived. Those for the arithmetic mean distance (AMD) and one for the arithmetic mean square distance (AMSD) seem to be new.

The paper lists the source code of a MATLAB® function to implement the formula on a computer, together with numerical examples. Further, the code for solving a coil design problem with constraints as it arises in practical engineering is presented, and an example problem is solved.

1. Introduction

Inductors are basic components of many electric and electronic devices. Nowadays, electronic circuits are produced as planar structures like microelectronic integrated circuits (IC's) and printed circuit boards (PCB's). Thus, inductors are often realized as planar spiral coils. This is the case in radio frequency integrated circuits (RFIC's) [1], in 13.56 MHz radio frequency identification (RFID) [2], near field communication (NFC) [3], and telemetry antennas [4], in wireless charging devices [5, 6], and as eddy current sensors for nondestructive testing [7, 8]. In these applications, the coils must be designed to a specified inductance. Hence, values of the design parameters resulting in the required inductance must be found.

This represents a simple form of an inverse problem. It can only be solved indirectly, by calculating the inductance of many coils, subject to any constraints, and by choosing the design whose inductance matches the predefined value best, e.g. using an optimization method. To do so, a method is needed to calculate the inductance of a coil from its design parameters. In principle, this can be done with the help of a field solver. In many cases, it suffices to know the low-frequency or direct current (DC) inductance (see sections 6 and 8). But even for designing a single inductor, creating the data file defining the layout is tedious, particularly if the coil has many windings, let alone if the calculation must be repeated for many different designs, as is the case in an inverse problem. Moreover, the computer run time may become very long. So, this way of solution is impractical.

The Greenhouse method [9] offers an analytical alternative. It allows precise calculations of the DC inductance. The method consists of dividing the coil into its constituent straight conductor segments and calculating their partial self-inductance and all mutual inductances between them separately, using analytical formulae and summing up all the contributions. But the method doesn't provide an inductance formula that explicitly depends on the design parameters, like the number of turns, the coil size, etc. Thus, for large numbers of turns and for solving inverse problems, the method becomes tedious.

Therefore, many researchers have worked on finding approximate inductance formulae that explicitly depend on the design parameters. Using such a formula is by far the easiest and fastest way to calculate coil inductance, particularly for solving inverse problems.

Some formulae approximating the DC inductance of planar spiral coils with rectangular conductor cross section are known from the literature, see ([8], equation (3)) and [10] where the maximum error of six of the most cited formulae are compared. Of these, only Crols et al.'s empirical formula [11] is applicable to any coil geometry, but the authors only discussed square and circular spiral coils. All other formulae are limited to square spiral coils. Whereas rectangular spiral coils were tested as eddy current sensors and a double-integral representation of the impedance of such coils was derived [7], in IC design only square spiral inductors seem to be have been considered until today ([12], section I). It appears to me that there should also be a case for using rectangular spiral coils in practical IC design, since they provide more flexibility for optimization under geometric constraints. This may even help to reduce cost. Jayaraman et al. argued along similar lines stating that "*A rectangular spiral outline shape allows flexibility to the designer while doing layout floor planning at the circuit level. Thus, the design and modeling of rectangular spiral inductors are of great interest to the circuit designers.*" ([12], section I).

Further, in designing inductors for RFID devices, it is imperative to be able to master rectangular spiral coils because the standard ISO 7810 prescribes the exact size of transponder cards, which is rectangular. To maximize the reading distance, their antennas must be made as large as possible. Hence, they must be rectangular. Consequently, also many RFID reader antennas are rectangular. This applies to many NFC devices as well, particularly to mobile phones, whose housing is rectangular.

Shortly before this paper was submitted, Jayaraman et al.'s work, the first paper presenting a formula for rectangular spiral coils based on physical principles came out [12]. They adapted Mohan's current sheet approximation for the DC inductance of square spiral coils [13] to rectangular ones and introduced some improvements. In the current sheet approximation, the coil is modeled as four homogeneous conductive sheets forming the four sides of the rectangle. The gaps between parallel conductor segments (see Fig. 1 for a typical layout) are ignored. For square coils, the maximum error of this approximation was found to be 29 % ([10], subsection 4.4). With the same method of error analysis and based on the same domain of definition, I have found the maximum error of Jayaraman et al.'s model ([12], equations (1) – (5)) to be 28 %.

For specific application areas, it is possible to reduce the domain of definition. This lowers the maximum error. The error analysis described in section 5 comprises a systematic variation of all design parameters of rectangular coils and exactly known inductances of close to 194000 designs. This analysis has revealed the following maximum errors of the model [12] for specific applications areas: 18 % for inductors in RFIC's, 14 % for RFID and telemetry reader antennas and NFC antennas, and 11 % for RFID and telemetry transponder antennas. These are all *maximum* errors. The individual error in a specific case may be substantially smaller. But for the circuit designer, only the maximum error counts because this is the error he or she must expect when designing a coil.

This paper derives a more precise formula. Its maximum error over the whole domain of definition amounts to 5.6 %, compared to 28 % of the model [12], and it lowers the maximum errors for the specific application areas listed above down to 2.3 %, 2.6 %, and 1.5 %, respectively.

Recently, an improved formula for square coils was presented [14]. It lowered the maximum error from hitherto 29 % down to 2.0 %. Therefore, it is sensible to try to adapt it to the rectangular case. Unfortunately, the two-dimensional empirical correction factor in the formula ([14], equation (25)) only holds for coil aspect ratios close to unity. For larger ratios, the correction fails. E.g. for a ratio of 5.0, the error can rise up to 120 %. But a closer inspection has revealed a systematic dependence of the error on four parameters. Hence, one could, in principle, derive a new correction factor adapted to the rectangular case. But it would require a four-dimensional fit instead of a two-dimensional one. This was deemed to be too involved.

Thus, an alternative solution was sought. It was found in the following approach: The conductor segments forming the spiral are connected in series, whereby the current remains constant along the spiral. So, as far as the mutual inductances between the parallel segments are concerned, the latter may as well be regarded as being connected in parallel. In a first step, this allows to model the spiral coil as a single-turn coil as in the current sheet approximation [12, 13], but with the essential difference that the four sides of the rectangle are not approximated as homogeneous conductors, but consist of N parallel conductor segments (N being the number of turns), so that the gaps between them are considered. Their mutual inductances are calculated similarly to the Greenhouse method [9], except that their individual lengths are approximated by their average length. This enables the inductance to be calculated with the help of the method of mean distances [15] by treating each side of the coil as one single conductor composed of N parallel conductor segments. The mean distances between two arbitrary points anywhere within the total cross section of the coil are then needed. These mean distances are composed of elementary ones of two types, firstly, between a single rectangle and itself, and secondly, between two displaced congruent rectangles. The method of mean distances relies on three kinds of mean distance: the geometric mean distance (GMD), the arithmetic mean square distance (AMSD), and the arithmetic mean distance (AMD). Finally, the inductance of the single-turn coil is then multiplied by N^2 to get the total inductance, exactly as in the current sheet approximation.

The resulting formula is purely based on physical principles and on approximations for the mean distances. The latter are found with the help of exact expressions that are derived in this paper. Unlike for the formula developed in [14] for square coils, no empirical correction factor for the inductance is needed. So, the formula is inherently scalable. Hence, it is valid for all coil dimensions and inductance ranges. For a proof see ([10], p. 39).

Section 2 defines the design parameters of rectangular planar spiral inductors. Section 3 explains the method of error analysis employed in validating the approximations for the mean distances. The derivation of the inductance formula is given

in section 4. Section 5 presents the error analysis of the inductance formula. A comparison with measurements is found in section 6. Section 7 discusses a MATLAB function for implementing the formula on a computer, together with numerical examples. Section 8 describes the automatic solution of an inverse problem with constraints to design a coil in an RFIC. An exemplary MATLAB code is given. Section 9 concludes i.a. that this paper provides the first experimentally verifiable evidence of the usefulness of the full method of mean distances as it was introduced in [15]. In the appendices 1 – 3, exact expressions for the GMD, AMSD, and AMD of rectangles are derived. Those for the AMD and one for the AMSD seem to be new. Appendix 4 lists the source code of the MATLAB function to evaluate the inductance formula.

2. Design parameters of planar spiral coils

Fig. 1 shows the layout of a rectangular planar spiral coil together with the definition of its dimensional design parameters. These are:

- N, number of turns or windings ($N \geq 2$).
- A, longer outermost mid-conductor side length.
- B, shorter outermost mid-conductor side length.
- A_{in}, longer innermost mid-conductor side length.
- B_{in}, shorter innermost mid-conductor side length.
- w, winding distance or -pitch ($w = s + g$).
- g, gap or spacing between windings.
- s, conductor width.
- h, conductor height or -thickness (hidden in Fig. 1).

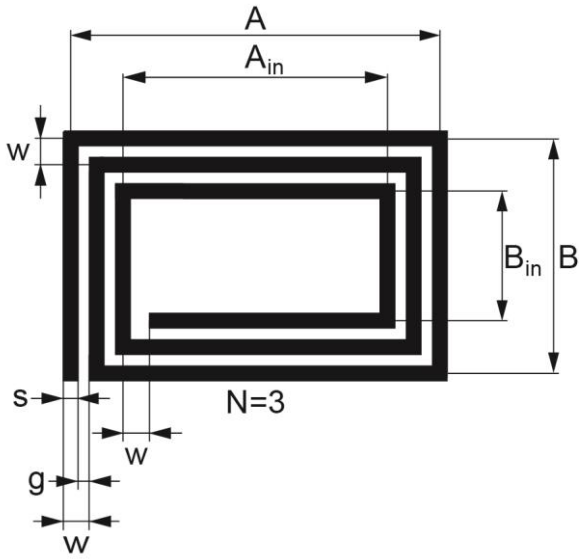

Figure 1: The layout of a rectangular planar spiral coil and its dimensional design parameters.

There is also a set of dimensionless parameters (see next section). Note that N, as a generic parameter, belongs to both sets. From Fig. 1, the following relations can be inferred:

$$A_{in} = A - 2(N-1)w, \qquad B_{in} = B - 2(N-1)w\,. \quad (1)$$

3. The method of error analysis

The derivation of the inductance formula implies testing approximations for the mean distances to choose the best ones. Of course, one could simply compare some values of approximated distances with exact values to assess the approximation. Exact expressions for all elementary mean distances are derived in appendices 1 – 3. But this would shed no light on the contribution of the approximation to the maximum error of the inductance formula. Depending on the design parameters, the calculated inductance may be insensitive to the error of the mean distance. Or, quite to the contrary, the result may be very sensitive to it, magnifying any relative error of the mean distance, e.g. if the self- and the mutual inductance terms are of comparable magnitude. Their difference is the total inductance, see equation (30). So, what one needs is a way to systematically test the effect of any such approximation on the maximum error of the inductance formula. These tests must include all dimensions of the parameter space and cover its whole domain of definition.

In a recent paper, a method of error analysis was developed for square coils, and exact inductance data for 13851 coil designs were compiled [10]. Besides its use for finding the maximum error of various inductance formulae, this method offers the very possibility to perform the tests needed. Therefore, this section provides an outline of the method.

For the purpose of assessing the quality of approximations, we may limit the analysis to the case of square coils. This is justified because square coils always have the largest maximum error, as will be shown in section 5.

Square planar spiral coils are characterized by five parameters, e.g. N, A, w, s, and h. Their number can be reduced to four by transforming them to dimensionless ones [10]. These are N, ρ, κ, and γ, in the order of importance in determining the inductance. The parameter $0 < \rho < 1$ is the filling factor. For a square coil, it is the ratio W/a of the overall width W spanned by one row of the N windings,

$$\mathrm{W} = \frac{[A + s - (A_{in} - s)]}{2} = (N-1)w + s, \qquad (2)$$

see Fig. 1 and equation (1), and the average conductor length

$$a = \frac{A + A_{in}}{2} = A - (N-1)w, \qquad (3)$$

yielding

$$\rho = \frac{(N-1)w + s}{A - (N-1)w}.$$

Now we modify this definition for the later use for rectangular coils. Without restricting generality, we may assume

$$A \geq B,$$

and we redefine ρ in terms of the shorter rectangle side, substituting B for A and B_{in} for A_{in} in equation (2). This leaves the result for W unchanged. Equation (3) is replaced by the equation for the shorter average conductor length

$$b = \frac{B + B_{in}}{2} = B - (N-1)w, \tag{4}$$

leading to $\rho = \mathrm{W}/b$ or

$$\rho = \frac{(N-1)w + s}{B - (N-1)w}. \tag{5}$$

A maximum value of ρ is allowed for any given combination of parameter values ([10], equation (19)). This is to prevent invalid parameter combinations, like e.g. a too large conductor width for the given coil dimension and number of windings, for which the length of the innermost conductor segment would vanish or even become negative ([10], p. 40). With definition (5), we are on the safe side because it yields larger values of ρ than the original definition. The remaining two dimensionless parameters besides N and ρ are the relative winding distance κ defined as

$$\kappa = \frac{w}{s} > 1,$$

and the cross-sectional aspect ratio γ,

$$\gamma = \frac{s}{h} \geq 1.$$

In PCB's, one has $\gamma \gg 1$. In RFIC's, values down to $\gamma = 2$ occur ([13], Table 4.10, $h = 0.9$ µm). Permitting $\gamma \geq 1$ also allows for square cross sections. The inverse transformation equations can be found in section 8.

The designs were defined by $A = B = 1$ mm and all parameter combinations given by the Cartesian products of the sets of values of the dimensionless parameters N, ρ, κ, and γ listed below. The parameter combinations are grouped in four ranges of N containing 1, 5, 5, and 8 values of N, and 9 values each of ρ, κ, and γ, resulting in a total of $(1 + 5 + 5 + 8) \cdot 9^3 = 729 + 3645 + 3645 + 5832 = 13851$ parameter combinations or coil designs. The exact inductances were calculated with the help of the free standard software FastHenry2 [16]. It can be downloaded from the site www.fastfieldsolvers.com. The calculations were done at DC, requesting 2×2 subfilaments. The conductivity of copper at 20 °C was used, i.e. $\sigma = 5.9595 \cdot 10^7\ \Omega^{-1}\mathrm{m}^{-1}$, corresponding to the resistivity $1/\sigma = 1.678 \cdot 10^{-8}\ \Omega\mathrm{m}$ ([17], $T = 293$ K). The sets of parameter sampling values for the four ranges of N were:

Two-windings range: $N = 2$,
$\rho = 0.01, 0.0537, 0.0975, 0.1412, 0.1850, 0.2288, 0.2725, 0.3162, 0.36.$

Low range: $N = 3, 4, 5, 6, 7$,
$\rho = 0.01, 0.0737, 0.1375, 0.2013, 0.2650, 0.3287, 0.3925, 0.4563, 0.52.$

Medium range: $N = 8, 9, 10, 11, 12$,
$\rho = 0.01, 0.1063, 0.2025, 0.2988, 0.3950, 0.4913, 0.5875, 0.6838, 0.78.$

High range: $N = 13, 14, 15, 16, 17, 18, 19, 20$,
$\rho = 0.01, 0.1162, 0.2225, 0.3287, 0.4350, 0.5413, 0.6475, 0.7538, 0.86.$

All ranges of N:
$\kappa = 1.1, 2.2125, 3.3250, 4.4375, 5.5500, 6.6625, 7.7750, 8.8875, 10.$
$\gamma = 1, 2.4, 5.6, 13.3, 31.6, 75, 177.8, 422, 1000.$

Note that the values of ρ differ from range to range. The reason is that, depending on N and κ, a maximum value of ρ is allowed (see the comment following equation (5)). In the lists above, the most restrictive upper limit for ρ that is valid for all κ and for all N within each range is used [10].

Now one can calculate the respective inductances with the formula in question, e.g. with the approximation for one of the mean distances, for the 13851 parameter combinations and compare the maximum relative error to the value obtained with the exact expression. This is done in the next section to select the best possible approximation for each of the mean distances.

4. Derivation of the inductance formula

In the spiral coil, the lengths of the parallel conductor segments forming the windings vary from $A_{in} - w$ to A and from B_{in} to B, respectively, see Fig. 1. In this derivation, the coil is approximated as a single-turn coil with N parallel conductor segments in each of its four sides. To enable the use of the method of mean distances [15], all segments on the same side are approximated to have the same average length a or b given by equations (3) and (4).

4.1. Precise expression for the partial self-inductances

According to the method of mean distances, the partial self-inductances L_a and L_b of the sides of length a and b, respectively, can be summarized in the form ([15], equation (33)):

$$L_\mathrm{c} = \frac{\mu_0 \mathrm{c}}{2\pi}\left[\log\left(\sqrt{\mathrm{c}^2 + {AMSD_L}^2} + \mathrm{c}\right) - \log GMD_L - \sqrt{1 + \left(\frac{AMSD_L}{\mathrm{c}}\right)^2} + \frac{AMD_L}{\mathrm{c}}\right], \tag{6}$$

where

$$\mathrm{c} = a, b.$$

Throughout this paper, log designates the natural logarithm. The constant μ_0 is the magnetic permeability of the vacuum, $\mu_0 = 4\pi \cdot 10^{-7}\ \mathrm{Vs/(Am)}$. The quantities $AMSD_L$, GMD_L, and AMD_L are the compound mean distances belonging to the partial self-inductances of the sides of the single-turn coil. They are the respective mean distances between two arbitrary points anywhere within the cross section of N parallel conductor segments, i.e. anywhere within a row of N congruent rectangles, see Fig. 2. So, these quantities represent compound mean distances spanning over N rectangles.

Equation (6) is very precise provided that the ratio $l/s \geq 1$, where l is the length of the conductor. The percentage error of the method of mean distances is plotted for a single straight wire of circular cross section as a function of the ratio l/R in ([15], Fig. 6), where R is the wire radius. The smaller this ratio, the larger is the error. To translate between circular and square cross section, note that we have $GMD_{circ} = 0.7788 \cdot R$ ([15], equation (15)) on one hand and $GMD_{square} = 0.4470 \cdot s$, equation (17), on the other hand. Hence, for a square cross section, the equivalent width amounts to $s = 1.7423 \cdot R$. Then the square and the circular cross section both have the same GMD.

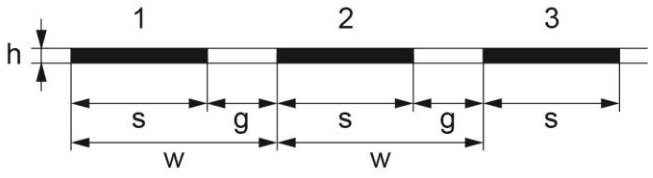

Figure 2: The cross section of $N = 3$ parallel conductor segments from Fig. 1.

The equivalent worst-case ratio l/R in a spiral coil is found in its shortest conductor segment. This is the innermost one. Its length is $l = A_{in} - w$, see Fig. 1. Hence, the equivalent ratio l/R of a conductor of square cross section corresponding to a round wire of the same length is $1.7423 \cdot (A_{in} - w)/s$. For the coil designs defined in section 3, its minimum value is 3.85 (attained for $N = 13$, $\rho = 0.86$, and $\kappa = 1.1$). According to ([15], Fig. 6), for $l/R = 3.85$, the error of the partial self-inductance obtained by the method of mean distances for circular cross section lies below 0.007 % if the exact values for the GMD, AMSD, and AMD are used. For square cross section, this is only an approximation. But it demonstrates that the use of the method of mean distances for planar spiral coils is well justified.
To apply it to calculate the partial self-inductances L_c according to equation (6), we need the compound mean distances GMD_L, $AMSD_L$, and AMD_L between the total cross-sectional area A_t and itself (drawn black in Fig. 2).

We start by calculating $\log GMD_L$. It is given by the double area integral ([18], equation (6.32), p. 273)

$$\log GMD_L = \frac{1}{|A_t|^2} \iint\limits_{A_t A_{t'}} \log(\delta)\, dA_t' dA_t\,,$$

where δ is the distance between any two points within the total surface $A_t' = A_t$ of total area $|A_t|$. Now, A_t is composed of N disjunct and congruent rectangles A_i of area $|A_i| = A = sh$, see Fig. 2. Hence, $|A_t| = NA$. By virtue of the linearity of the integral, the double area integral over A_t and $A_t{}'$ can be expressed as the double sum of N^2 double area integrals over the rectangles A_i and A_j. Thus,

$$\log GMD_L = \frac{1}{N^2} \sum_{i=1}^{N} \sum_{j=1}^{N} \frac{1}{A^2} \iint\limits_{A_i\, A_j} \log\left(\delta_{i,j}\right) dA_j dA_i\,, \quad (7)$$

where $\delta_{i,j}$ is the distance between one integration point located in rectangle A_i and the other one in rectangle A_j.
Two cases can be distinguished: The two integration points either lie in the same rectangle (case 1) or in different ones (case 2). Hence, the double sum (7) can be split into two parts representing the two cases, $\log GMD_{L,1}$ and $\log GMD_{L,2}$:

$$\log GMD_L = \log GMD_{L,1} + \log GMD_{L,2}. \quad (8)$$

In case 1, only the summands with $i = j$ are extracted from the double sum (7) to form $\log GMD_{L,1}$. It reduces to the sum of N identical contributions, which, by definition, are all given by the logarithm of the elementary GMD between a single rectangle and itself, denoted by $\log GMD_1$, normalized by $1/N^2$. Hence,

$$\log GMD_{L,1} = \frac{1}{N^2} N \log GMD_1\,. \quad (9)$$

The exact expression for $\log GMD_1$ is presented in appendix 1, equation (39).
In case 2, only the summands with $i \neq j$ are extracted from the double sum (7) to form $\log GMD_{L,2}$. It represents the sum of the remaining $N(N-1)$ contributions, which, by definition, are given by the logarithm of the elementary GMD between two rectangles displaced by a multiple k of the winding distance w, denoted by $\log GMD_2\,(kw)$, normalized by $1/N^2$. By contrast with case 1, here the contributions are not all equal, but they depend on the multiplier k. Hence, the second part of the double sum (7) must be transformed to a single sum with k as the summation index.
In Fig. 2 there are three pairs of rectangles: Two pairs, $(1,2)$ and $(2,3)$, each have the displacement w, and one pair, $(1,3)$, has the displacement $2w$. So, $k = 1 \ldots 2$. For N windings this becomes $k = 1 \ldots N-1$ because there are $N-1$ gaps between N rectangles. Thus, the largest displacement of two rectangles is $(N-1)w$. For each value of k, there are $N-k$ pairs of rectangles of mutual displacement kw. Each of these pairs must be counted *twice*, because in the double sum (7), all pairs with $i \neq j$ occur twice: once as (i,j), and once as (j,i), and both notations refer to the same pair. Hence, the second part of the double sum (7) transforms to

$$\log GMD_{L,2} = \frac{2}{N^2} \sum_{k=1}^{N-1} (N-k) \log GMD_2\,(kw)\,. \quad (10)$$

The exact expression for $\log GMD_2$, the logarithm of the elementary GMD between two displaced rectangles, is given in appendix 1, equation (38). The total number of contributions in case 2 is

$$2\sum_{k=1}^{N-1}(N-k) = 2(N-1)N - 2\sum_{k=1}^{N-1}k = N(N-1) \quad (11)$$

as anticipated above, confirming the correctness of the transformation leading to the single sum (10). With the help of equations (9) and (10), the sum (8) becomes

$$\log GMD_L = \frac{1}{N^2}\left[N \log GMD_1 + 2\sum_{k=1}^{N-1}(N-k)\log GMD_2\,(kw)\right]. \quad (12)$$

Next, the quantity ${AMSD_L}^2$ in equation (6), i.e. the square of the compound AMSD belonging to the partial self-inductances of the sides of the coil, is defined analogously to equation (7) as

$${AMSD_L}^2 = \frac{1}{N^2}\sum_{i=1}^{N}\sum_{j=1}^{N}\frac{1}{A^2}\iint_{A_i\,A_j}{\delta_{i,j}}^2\,dA_j dA_i. \quad (13)$$

Analogously to equation (12), by the definition of ${AMSD_1}^2$, the square of the elementary AMSD between a single rectangle and itself, and ${AMSD_2}^2$, the square of the elementary AMSD between two displaced rectangles, one obtains

$${AMSD_L}^2 = \frac{1}{N^2}\left[N \cdot {AMSD_1}^2 + 2\sum_{k=1}^{N-1}(N-k){AMSD_2}^2\,(kw)\right]. \quad (14)$$

The exact expressions for ${AMSD_1}^2$ and ${AMSD_2}^2$ are presented in appendix 2, equations (43) and (42), respectively.

Finally, the quantity AMD_L in equation (6), i.e. the compound AMD belonging to the partial self-inductances of the sides of the coil, is defined analogously to equation (13) as

$$AMD_L = \frac{1}{N^2}\sum_{i=1}^{N}\sum_{j=1}^{N}\frac{1}{A^2}\iint_{A_i\,A_j}\delta_{i,j}\,dA_j dA_i. \quad (15)$$

Analogously to equation (14), by the definition of AMD_1, the elementary AMD between a single rectangle and itself, and AMD_2, the elementary AMD between two displaced rectangles, one obtains

$$AMD_L = \frac{1}{N^2}\left[N \cdot AMD_1 + 2\sum_{k=1}^{N-1}(N-k)AMD_2\,(kw)\right]. \quad (16)$$

The exact expressions for AMD_1 and AMD_2 are derived in appendix 3, equations (48) and (46), respectively.

Now the exact expressions for all quantities appearing in equation (6) are known, and the partial self-inductances L_a and L_b can be evaluated.

4.2. Approximate expression for the partial self-inductances

The equations derived in subsection 4.1 for the compound mean distances spanning over several rectangles and the expressions for the elementary mean distances derived in the appendices are exact. Only equation (6) is not exact, although it is very precise, see subsection 4.1. The resulting formulae get very complicated. But since the concept of average-sized single-turn coil is only a rather coarse approximation for the spiral coil, it is not worth evaluating them exactly. Instead, good approximations would be useful.

The method of error analysis from section 3 allows to assess the effect of approximations on the maximum error of the inductance formula over the whole domain of definition of the design parameters of square coils. In this and the next subsection, the method is used to validate approximations for the equations appearing in subsection 4.1.

The first equation that might be simplified is equation (6), since the mean distances AMSD and AMD are often neglected altogether, see e.g. in ([14], equation (2)). This is viable when the mean distances only stretch across a single conductor, i.e. a single rectangle in Fig. 2. But here they span over all N rectangles. An error analysis according to section 3 revealed that neglecting the mean distances $AMSD_L$ and AMD_L in equation (6) in the final version of the inductance formula as defined in subsection 4.4 raised the maximum error to 30 % ($N = 13$, $\rho = 0.86$, $\kappa = 2.2125$, and $\gamma = 1.0$). Thus, the AMSD and AMD cannot be neglected.

Another simplification of equation (6) often found in the literature is substituting both the AMSD and the AMD by the GMD, so that only the latter needs to be calculated. An analogous error analysis disclosed a maximum error of 14 % (as above, but $\kappa = 10.0$). So, this simplification is not an option either. Hence, equation (6) cannot be simplified.

Seeking approximations for the mean distances was more successful. Rosa ([19], p. 314) and Grover ([20], p. 22) showed that the GMD between a single rectangle (of width s and height h) and itself, whose exact expression is given in equation (39), can be approximated as

$$GMD_1 \approx 0.2235(s+h) \quad (17)$$

or

$$\log GMD_1 \approx \log(s+h) - 3/2\,. \quad (18)$$

For the coil designs in section 3, an error analysis showed that, if in the final version of the inductance formula as defined in subsection 4.4, equation (18) was substituted by the exact expression (39) in equation (12), the maximum error changed by not more than 0.05 %. Therefore, approximation (18) is validated.

The exact expression (38) for the GMD between two displaced congruent rectangles is even more complicated than equation (39), so an approximation is even more desirable. The only approximation found in the literature was the one derived by Rosa ([21], equation (13)) as the series expansion

of the exact solution for the GMD between two axially displaced line segments of equal length s. This is the special case of two congruent rectangles of vanishing height $h = 0$, and for the displacement $w = ns$, $n \in \mathbb{N}$:

$$\log GMD_2 \approx \log ns - \left(\frac{1}{12n^2} + \frac{1}{60n^4} + \frac{1}{168n^6} + \cdots\right),$$

which corresponds to $\kappa = w/s = n \in \mathbb{N}$. It converges very fast except for $n = 1$. It can also be found in ([20], p. 20). Rosa's derivation [21] remains valid for $\kappa \in \mathbb{R}$, so Mohan wrote it in the generalized form ([13], equation (3.13))

$$\log GMD_2 \approx \log w - \left(\frac{1}{12\kappa^2} + \frac{1}{60\kappa^4} + \frac{1}{168\kappa^6} + \cdots\right).$$

This formula was adopted with the same number of terms by Jayaraman et al. in their recent paper ([12], equation (3)).
By contrast, equation (20) will consider the finite height h of the rectangles, thus extending the applicability of the inductance formula to coils with low $\gamma = s/h$ down to $\gamma = 1$. Not surprisingly, an error analysis according to section 3 showed that, if in the final version of the inductance formula as defined in subsection 4.4, equation (20) was replaced by the GMD between two displaced line segments, the maximum errors in the four ranges of N worsened from
4.3 %, 3.1 %, 3.7 %, and 5.6 %
to
6.0 %, 5.1 %, 3.6 %, and 5.4 %.
Because of this large increase of up to 2.0 %, equation (20) was preferred.
To derive equation (20), one can guess that $\log GMD_2$ should also depend on $\log(s + h)$, as $\log GMD_1$ does, since for zero displacement $w = 0$, the rectangles coincide: $GMD_2 = GMD_1$. Further, GMD_2 must depend on w. Intuitively, one may expect it to depend on the relative displacement $\kappa = w/s$. Indeed, some trial calculations revealed that for *square* cross section, $h = s$, $\log GMD_2$ was very well approximated by

$$\log GMD_2 \approx \log(s + h) + \log\left(\frac{\kappa}{2}\right). \qquad (19)$$

So, despite the intuition that leads to equation (19), it is not even defined for $w = 0$. Interestingly, for $h = s$, this is identical to $\log w$, the first term of the series expansion for the GMD between two displaced line segments (which is based on $h = 0$). In the general case of *rectangular* cross section, $\log GMD_2$ must also depend on the cross-sectional aspect ratio $\gamma = s/h$. Although approximation (19) does depend on h, it is only valid for square cross section, $\gamma = 1$. It had to be extended to cover the case $\gamma > 1$. Plotting the exact solution of $\log GMD_2(\kappa)$ according to equation (38) for various values of γ, together with the approximation (19), both as a function of κ, always resulted in a nearly constant difference between the two plots. This meant that the required correction mainly depended only on γ, but not on κ. Hence, it sufficed to add a function of γ to equation (19) fitting this difference to arrive at the general approximation. Least-squares fits of various types of elementary functions revealed a rational function as the best fit for values of γ in the interval $[1.0, 1000]$. The resulting approximation for $\log GMD_2$ was

$$\log GMD_2 \approx \log(s + h) + \log\left(\frac{\kappa}{2}\right) - \frac{-1.46\gamma + 1.45}{2.14\gamma + 1}. \qquad (20)$$

For $\gamma \approx 1$, the correction in γ vanishes, as expected. An error analysis according to section 3 showed that, if in the final version of the inductance formula as defined in subsection 4.4, equation (20) was substituted by the exact expression (38) in equation (12), the maximum errors in the four ranges of N changed by 0.11 % maximum. Hence, approximation (20) is well-founded.

Next, the exact expression (43) for ${AMSD_1}^2$ in equation (14) is so simple that it doesn't need an approximation:

$${AMSD_1}^2 = \frac{1}{6}(s^2 + h^2).$$

In the exact expression (42) for ${AMSD_2}^2$, the square terms beside w^2 can even be neglected, so it simplifies to

$${AMSD_2}^2 \approx w^2, \qquad (21)$$

affecting the maximum error of the inductance formula by less than 0.009 %.

Finally, the exact expression (48) for AMD_1 in equation (16) is as complicated as equation (39) for $\log GMD_1$, so an approximation would be helpful. In his dissertation, Mohan suggested the formula ([13], equation (3.21))

$$AMD_1 \approx \frac{\sqrt{s^2 + h^2 + 0.46sh}}{3},$$

indicating a precision of 2 %, but without disclosing how he had found the formula and against what reference he had calculated the error. I found a maximum error of 1.4 % compared to the exact expression (48) for a ratio s to h (or vice versa) close to 5.12. Note that the formula above is symmetrical on exchanging s and h, as it must be. Hence, its error only depends on the ratio of s and h.
In the literature, the AMD is often approximated by the GMD. In our case this means

$$AMD_1 \approx GMD_1, \qquad (22)$$

where GMD_1 is given in equation (17). An error analysis based on section 3 revealed that, if in the final version of the inductance formula as defined in subsection 4.4, the exact expression (48) was substituted for equations (22) and (17) in equation (16), the maximum error changed by 0.15 % maximum. Therefore, approximation (22) is justified. If Mohan's formula was used instead of equation (22), the maximum error in the lower ranges of N increased by 0.15 %, so equation (22) was preferred.

The exact expression (46) for AMD_2 is very complicated. An approximation was needed. Here as well, the approximation

$$AMD_2 \approx GMD_2 \tag{23}$$

can be made. GMD_2, in turn, can be approximated by taking the exponential function of expression (20). Substituting the exact expression (46) for equation (23) and the exponential function of expression (20) in equation (16) changed the maximum error of the calculated inductance by less than 0.09 %. So, approximation (23) is viable.
Note that applying equations (22) and (23) is *not* the same as setting $AMD_L \approx GMD_L$. This would result in a maximum error of 16 % ($N = 13$, $\rho = 0.86$, $\kappa = 10.0$, and $\gamma = 1.0$).

4.3. Approximate expression for the mutual inductances

The mutual inductance M_a between the two rows of parallel conductors of average length a at average mutual distance b, and the mutual inductance M_b between the other two rows of parallel conductors of average length b at average mutual distance a, are given by an equation analogous to (6),

$$M_{\mathfrak{c}} = \frac{\mu_0 \mathfrak{c}}{2\pi}\left[\log\left(\sqrt{\mathfrak{c}^2 + AMSD_{\bar{\mathfrak{c}}}{}^2} + \mathfrak{c}\right) - \log GMD_{\bar{\mathfrak{c}}} - \sqrt{1 + \left(\frac{AMSD_{\bar{\mathfrak{c}}}}{\mathfrak{c}}\right)^2} + \frac{AMD_{\bar{\mathfrak{c}}}}{\mathfrak{c}}\right], \tag{24}$$

where

$$\mathfrak{c} = a, b\,,$$
$$\bar{\mathfrak{c}} = b, a.$$

If $\mathfrak{c} = a$, then $\bar{\mathfrak{c}} = b$, and vice versa.

We start by calculating $\log GMD_{\bar{\mathfrak{c}}}$, the logarithm of the compound GMD between two rows of rectangles that are in-line. The cross-sectional view of the spiral coil with the two rows of rectangles is exemplified in Fig. 3.

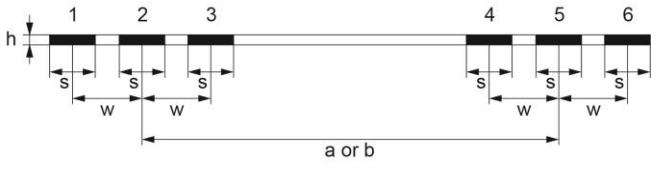

Figure 3: The total cross section of the coil from Fig. 1.

In calculating $\log GMD_{\bar{\mathfrak{c}}}$, the two integration points always lie in two different rectangles. One of the points lies in a rectangle in the left row (i.e. in one of the rectangles 1, 2, or 3 in Fig. 3), and the other one in a rectangle in the right row (i.e. in one of the rectangles 4, 5, or 6). So, analogously to equation (7), we have a double sum of N^2 double area integrals,

$$\log GMD_{\bar{\mathfrak{c}}} = \frac{1}{N^2}\sum_{i=1}^{N}\sum_{j=N+1}^{2N}\frac{1}{A^2}\iint_{A_i A_j}\log\left(\delta_{i,j}\right) dA_j dA_i\,. \tag{25}$$

In the double sum (25), only contributions of case 2 arise, namely, by definition, $\log GMD_2(\bar{\mathfrak{c}} + kw)$, normalized by $1/N^2$, where $k = -(N-1) \ldots (N-1)$, as can be inferred from Fig. 3. Since they depend on the multiplier k, we need an analogous transformation to a single sum with k as the summation index as in subsection 4.1. For each value of k, there are $N - |k|$ pairs of rectangles of mutual displacement $\bar{\mathfrak{c}} + kw$. In the double sum (25), none of the pairs of rectangles occurs twice, so there is no factor 2 in the resulting single sum. Hence, the double sum (25) transforms to

$$\log GMD_{\bar{\mathfrak{c}}} = \frac{1}{N^2}\left[\sum_{k=-(N-1)}^{N-1}(N-|k|)\log GMD_2(\bar{\mathfrak{c}} + kw)\right]. \tag{26}$$

The total number of pairs of rectangles is

$$\sum_{k=-(N-1)}^{N-1}(N-|k|) = 2\sum_{k=1}^{N-1}(N-k) + N\,.$$

With the help of equation (11), this is found to be N^2, consistent with the number of N^2 summands in equation (25), thus confirming the correctness of the transformation leading to the single sum (26).
The quantity $\log GMD_2$ could, in principle, be evaluated with the help of the exact expression (38). But for such large displacements compared to s and for $\gamma > 1$, expression (38) became numerically unstable. It then contained differences of numbers that were nearly equal, so that double precision arithmetic was not precise enough to represent them. This led to large errors beyond bound. So, equation (38) cannot be used to calculate $\log GMD_{\bar{\mathfrak{c}}}$.
A remedy might be to reformulate equation (38) in terms of ratios h/w, $h/(w+s)$, etc., and to derive a Taylor series expansion for small values of these ratios where, hopefully, the terms causing the instability would cancel analytically. Both types of functions occurring in equation (38), namely, $\log(1+x^2)$ and $\arctan(x)$, have alternating Taylor series, allowing the estimation and thus the control of the truncation error.
But it turned out that this tedious procedure is probably not worth the effort. It was possible to bypass the instability problem of equation (38) and to do the error analysis by restricting it to the subdomain characterized by $\gamma = 1$. It revealed that the maximum error of the inductance formula over all four ranges of N defined in section 3 changed by less than 0.0002 % if the approximation given in equation (27) was replaced by the exact expression (38). Due to this marginally small effect of approximation (27) for $\gamma = 1$, it may be expected to remain negligible for all $\gamma > 1$, even if it should increase by up to three orders of magnitude.
Two alternatives for approximating equation (38) were at hand: equation (20) with $\kappa = (\bar{\mathfrak{c}} + kw)/s$ and the central filaments approximation. In the latter, the GMD of the two conductor segments is simply replaced by their central distance $\bar{\mathfrak{c}} + kw$. One important result of the error analysis to be

discussed in section 5 is that the maximum error strictly decreases as a function of the coil aspect ratio

$$\Gamma = \frac{A}{B} \geq 1 \,.$$

Now, error calculations showed that equation (20) would confine this desirable property to within a narrower interval of Γ than the central filaments approximation, i.e. it would undesirably restrict the scope of applicability of error interpolation. Hence, in the calculation of the mutual inductances, the central filaments approximation was preferred, even though in the low range of N and at $\Gamma = 1$, the maximum error increased by $0.4\,\%$ compared to using equation (20). Therefore, equation (26) becomes

$$\log GMD_{\bar{\mathfrak{c}}} = \frac{1}{N^2}\left[\sum_{k=-(N-1)}^{N-1} (N-|k|)\log(\bar{\mathfrak{c}} + kw)\right], \quad (27)$$

with $\bar{\mathfrak{c}} = b, a$, see equation (24).

Next, in the analogous calculation of ${AMSD_{\bar{\mathfrak{c}}}}^2$ in equation (24), no instability problem arose, so the exact equation (42) for ${AMSD_2}^2$ could be used, substituting $\bar{\mathfrak{c}} + kw$ for w. Since $\bar{\mathfrak{c}} \gg w$, approximation (21) is even more justified in equation (24) than it was in equation (6). Thus, analogously to equation (27), one finds

$${AMSD_{\bar{\mathfrak{c}}}}^2 = \frac{1}{N^2}\left[\sum_{k=-(N-1)}^{N-1} (N-|k|)\,(\bar{\mathfrak{c}} + kw)^2\right]. \quad (28)$$

Finally, in the calculation of $AMD_{\bar{\mathfrak{c}}}$, the same problem as for $\log GMD_{\bar{\mathfrak{c}}}$ arose: The exact equation (46) for AMD_2 became numerically unstable. The problem was circumvented in the same manner, by applying the central filaments approximation, i.e. the exact AMD was simply replaced by the displacement $\bar{\mathfrak{c}} + kw$ as the only alternative available. Analogously to equation (28), this becomes

$$AMD_{\bar{\mathfrak{c}}} = \frac{1}{N^2}\left[\sum_{k=-(N-1)}^{N-1} (N-|k|)(\bar{\mathfrak{c}} + kw)\right]. \quad (29)$$

Here, an error analysis restricted to $\gamma = 1$ led to the same conclusion as for equation (38): It is probably not worth expanding equation (46) in a Taylor series. In the highest range of N , it remained numerically unstable, even for $\gamma = 1$.

4.4. The inductance formula

Finally, the inductance of the single-turn coil must be multiplied by N^2 to consider the effect of the windings, just as in the current sheet approximation [12, 13]. The total inductance L of the spiral coil then reads

$$L = 2N^2[L_a + L_b - (M_a + M_b)]\,, \quad (30)$$

where L_a and L_b are given in equation (6), which, in turn, refers to equations (3), (4), (12), (14), (16) – (18), (20) – (23), and (43), and M_a and M_b are defined in equation (24), which, in turn, refers to equations (3), (4) and (27) – (29). The factor 2 results from the fact that there are two sides of the rectangle with conductors of length a and two of length b, each having the partial self-inductance L_a and L_b, respectively, and that the mutual inductances M_a and M_b must be counted twice to consider the coupling from the conductors on one side of the rectangle to those on the opposite side, and vice versa.
One might argue here that the exponent of N in equation (30) should be < 2.0 since the size of the loops differs from turn to turn, leading to coupling losses resulting in a lower inductance. But this effect is already considered in the mean distances used in equations (6) and (24). Indeed, an error analysis according to section 3 confirmed that 2.0 is the optimum value.

5. Error analysis for rectangular coils

In the present work, to ensure comparability with the results from [10] and [14], the error analysis was done in the same way as described in [10] by varying all four dimensionless parameters N, ρ, κ, and γ and by using the same sampling values for the parameters. But the formulae derived in section 4 extend the scope of applicability to rectangular coils. So, a fifth dimensionless parameter had to be added, namely, the coil aspect ratio $\Gamma = A/B \geq 1$. The assumption $\Gamma \geq 1$ does not restrict generality, but it is necessary for the unambiguous and safe definition of ρ, see the comment following equation (5). For all ranges of N, the following 14 sampling values of Γ were used:

$$\Gamma = 1, 1.1, 1.25, 1.5, 1.75, 2, 2.25, 2.5, 2.75, 3, 3.25, 3.5, 3.75, 4.$$

The coil designs were defined by $B = 1$ mm and, for each of the four ranges of N, by all parameter combinations given by the Cartesian product of the respective sets of sampling values of the four dimensionless parameters N, ρ, κ, and γ presented in section 3, and the set of 14 sampling values of Γ listed above. Hence, the number of reference coil designs increased from 13851 in section 3 to $14 \cdot 13851 = 193914$.
A python script was used to automatically call the software FastHenry2 repeatedly for calculating the exact inductances of the reference coils. On a PC with a Xeon W-2125 processor (4 cores, 4 GHz) and 64 GByte random-access memory, the runtimes summed up to 22.8 hours. The MATLAB function listed in appendix 4 completed the calculations within 10.8 seconds.
The maximum errors over N, ρ, κ, and γ were calculated as a function of Γ up to $\Gamma = 10.0$. They were found to strictly decrease with increasing Γ in all four ranges of N, but only up to a certain limit. Beyond this limit, the error increased, and eventually its behavior even became chaotic. The said limit occurred earliest in the high range of N, at $\Gamma = 2.5$, and latest in the two-windings range, at $\Gamma = 4.0$. The results are listed in Table 1 as a function of Γ up to $\Gamma = 4.0$. Values beyond the limit of strict decrease are printed in red. The results

are also plotted in Figs. 4 – 7 as a function of Γ up to the limit of strict decrease. Note that every value in Table 1 and every point in Figs. 4 – 7 represents the maximum error of 729, 3645, 3645, and 5832 coil designs, respectively, depending on the range of N, over the domain of definition of ρ, κ, and γ as defined in section 3, computed at the respective value of Γ.

The property of strictly decreasing maximum error as a function of Γ was considered highly desirable. It allows to safely estimate the maximum error to be expected for any coil design by linear interpolation for any value of Γ below the limit of strict decrease. Consequently, the largest errors occur for square coils, i.e. at $\Gamma = 1$. This fact has already been exploited in section 4, as explained in section 3, and it will again be evoked in section 6.

For $\Gamma > 1$, the maximum errors decrease rapidly. The higher the range of N, the faster the maximum error decreases. The values of Γ at which it has halved are roughly 2.5, 2.25, 1.5, and 1.2, respectively, for the four ranges in increasing order of N.

The formula can be used up to $\Gamma = 4.0$ for all ranges of N, but interpolation of the maximum error is restricted to below the upper limit of strict decrease, i.e. to within the region with black numbers in Table 1. The region with red numbers displays chaotic behavior in the mid and high range of N.

The overall maximum error of 5.55 % is considerably larger than the value to be expected from the approximations used for the mean distances in section 4, where the largest contribution to the maximum error amounted to 0.4 % (see the comment preceding equation (27)). In addition, from the results obtained by the error analyses in section 4, it is evident that the contributions from the method of mean distances and from the central filaments approximation are marginal. All this suggests that the main contribution to the error of the inductance formula does not stem from these approximations, but rather from the concept of average-sized single-turn coil on which it is based, which approximates the varying lengths of the conductor segments by their averages a and b.

Table 1: The maximum relative errors of the inductance formula (30) for the four ranges of N defined in section 3, as a function of the coil aspect ratio Γ. Values beyond the limit of strict decrease are printed in red.

Γ	Two-wind. [%]	Low [%]	Mid [%]	High [%]
1.00	4.32	3.08	3.74	5.55
1.10	4.15	2.70	2.35	3.56
1.25	3.83	2.27	1.95	2.18
1.50	3.32	2.02	1.83	1.90
1.75	2.92	1.74	1.68	1.76
2.00	2.63	1.64	1.54	1.60
2.25	2.35	1.50	1.45	1.51
2.50	2.16	1.35	1.31	1.38
2.75	1.98	1.22	1.21	1.46
3.00	1.83	1.13	1.15	1.41
3.25	1.69	1.05	1.08	1.16
3.50	1.57	0.98	1.61	1.44
3.75	1.50	1.03	1.06	1.06
4.00	1.43	1.05	2.20	1.94

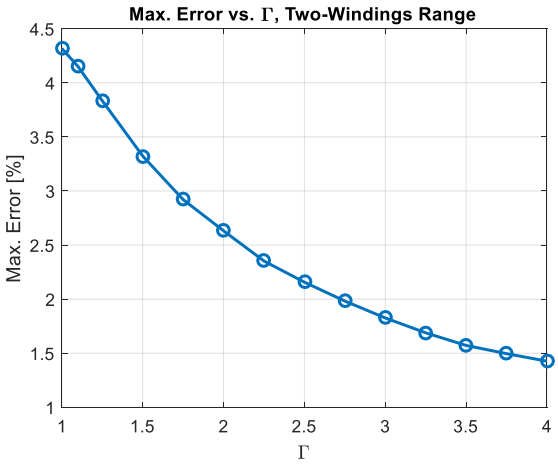

Figure 4: The maximum error of the inductance formula (30) as a function of Γ for the two-windings range, $N = 2$.

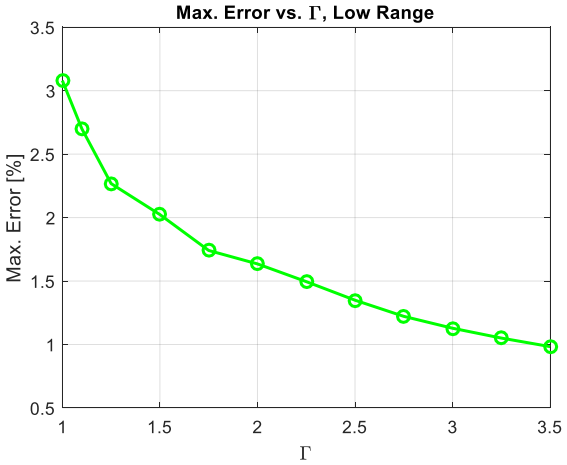

Figure 5: The maximum error of the inductance formula (30) as a function of Γ for the low range, $N = 3 \ldots 7$.

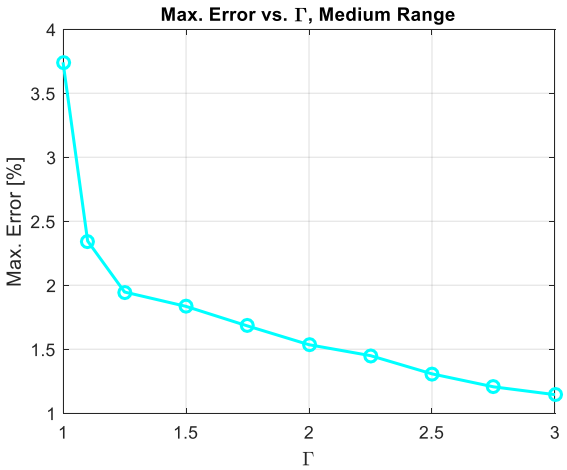

Figure 6: The maximum error of the inductance formula (30) as a function of Γ for the medium range, $N = 8 \ldots 12$.

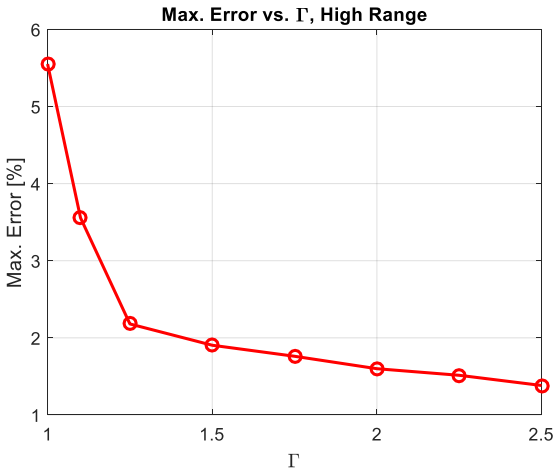

Figure 7: The maximum error of the inductance formula (30) as a function of Γ for the high range, $N = 13 \ldots 20$.

Therefore, avoiding this approximation would improve the accuracy. But fortunately, there is a simpler although partial solution: Restricting the domain of definition in three ways, depending on the field of application, allows the maximum error to be considerably reduced:

1. For RFIC's, useful restrictions are $N \geq 3$ and $\Gamma \geq 1.25$. According to Table 1, this reduces the maximum error to 2.3 %.

2. For RFID and telemetry reader antennas and for NFC antennas, meaningful restrictions are $N \leq 7$ and $\rho < 0.15$ ([10], p. 46). This reduces the maximum error to 2.6 %.

3. For RFID and telemetry transponder antennas[1], the restrictions $3 \leq N \leq 7$ ([10], p. 42) and $\rho < 0.15$ ([10], p. 46) are sensible. This reduces the maximum error to 1.5 %.

For wireless charging devices, as things stand now, one is free to choose the shape of the coils. In eddy current sensors, the strongest normalized impedance response was found for square coils [8]. Hence, for these application fields, square coils and the formula in [14] are recommended[2]. The latter features a maximum error of 2.0 %, compared to 5.55 % for equation (30) at $\Gamma = 1$.
With the reduced maximum errors resulting from the subdomains defined above, the inductance formula (30) is certainly precise enough to be used in circuit design. Note that it also holds for $N > 20$ with $\rho \leq (N-1)/(N+1)$ ([10], equation (20b)) for $\kappa \in [1.1, 10]$ and $\gamma \epsilon [1.0, 1000]$.

6. Comparison with measurements

The error analysis in the last section revealed that the largest errors of the inductance formula (30) arise for square coils. Therefore, it made sense to test the formula against measurements on coils with $\Gamma = 1$. So far, measurements seem to have been limited to inductors in RFIC's [10 – 13]. By contrast, in this section, measurements on 16 square RFID reader antennas manufactured as PCB's with standard copper layer thickness $h = 35$ µm are reported. They were performed at 300 kHz (representing DC, justified for 13.56 MHz in ([14], section 5)) with an Agilent® 4294A Precision Impedance Analyzer and an 42941A Impedance Probe.
Table 2 lists the 16 reader antennas, characterized by their design parameters N, A, w, and s, together with the measured inductances L_{meas} and the percentage deviations of the results of the inductance formula (30) from the measurements and from the exact values. The parameters w and s are given in mils, whereby 1 mil corresponds to 25.4 µm.

Table 2: Dimensional design parameters and measured inductances L_{meas} of 16 square reader antennas manufactured as standard PCB's ($h = 35$ µm), with the relative deviations of the inductance formula (30) from the measurements (Dev. 1) and from the exact values (Dev. 2).

N	A [mm]	w [mil]	s [mil]	L_{meas} [nH]	Dev. 1 [%]	Dev. 2 [%]
3	20	12	6	543	0.49	0.25
3	20	20	6	485	0.22	0.67
3	20	30	6	435	0.02	1.04
3	20	40	6	390	1.62	1.36
3	20	30	12	405	0.94	0.90
3	50	12	6	1719	0.02	0.07
3	50	20	6	1583	0.03	0.29
3	50	40	6	1384	0.21	0.58
3	50	20	12	1512	0.10	0.01
3	50	30	12	1397	0.32	0.33
3	50	40	12	1309	0.73	0.52
4	50	40	12	2042	1.01	0.66
5	50	40	12	2860	1.07	0.81
3	100	40	12	3177	0.41	0.28
5	10	12	6	448	1.64	1.03
3	50	30	18	1352	0.48	0.10

According to Fig. 10-6 of the operation manual of the measurement equipment, the measurement error at 300 kHz was less than 1 % for inductances above about 1 µH, and less than 3 % below. The maximum relative deviation of the inductance formula from the measured values was 1.64 % with a respective measurement error of 3 %. For the inductances above 1 µH with a respective measurement error of 1 %, the largest deviation was 1.07 %. The maximum deviation of the formula from the exact values amounted to 1.36 %, in agreement with the error analysis in section 5, which disclosed a maximum error of 1.5 % for $3 \leq N \leq 7$ and $\rho < 0.15$.

[1] Note that for coils made of *round* wire, which is often used for transponders antennas, other formulae for the mean distances apply. They can all be found in [15].

[2] Note that the formula in [14] is optimized for a slightly different layout than the one used here, compare Fig. 1 and ([14], Fig. 1).

7. Implementation in MATLAB

The source code of the MATLAB function `L_RectPlanarSpiral` to calculate the DC inductance of rectangular planar spiral coils is listed in appendix 4. All quantities are in SI units. Besides the inductance L, the function also returns the filling factor ρ given in equation (5). If the data entered represents an invalid parameter combination as explained in section 3, an error message is output. The invalid entry is detected by checking the value of ρ. Following are examples to test the correct implementation of the code. The data

```
A = 0.1; B = 0.05; w = 1e-3; s = 5e-4; h = 35e-6;
```

were used for all ranges of N. The MATLAB function is run by the command

```
[L, rho] = L_RectPlanarSpiral (N, A, B, w, s, h)
```

For each of the four ranges of N, Table 3 lists the number of windings N to be used in the test, the value of L returned by the MATLAB function, the exact DC inductance (from FastHenry2), the relative error of L, and the value of ρ returned.

Table 3: Example data for testing the MATLAB function presented in appendix 4.

N	L [μH]	L_{exact} [μH]	Err. [%]	ρ
2	1.064	1.063	0.13	0.0306
5	4.785	4.768	0.34	0.0978
10	13.525	13.398	0.94	0.2317
15	22.624	22.311	1.41	0.4028

8. Solving inverse problems

The following example shows how to solve inverse problems of coil design with constraints as they typically arise in electrical engineering. The example comprises the design of an RFIC inductor, but the same procedure can easily be adapted to any field of application.

The coil is to be etched on the top layer of a 0.35 µm complementary metal-oxide semiconductor (CMOS) process. Let the thickness of the layer be $h = 0.9$ µm. Suppose we dispose of an area of 150 µm × 250 µm which is not to be exceeded. Let the minimum permitted conductor width and gap between conductors be 1.0 µm. We want an inductance of 84.0 nH, and N shall be as small as possible to keep the loss resistance small.

What values of N, A, B, w or g, and s do we need? The straightforward way of solution would be to vary these dimensional parameters within the whole domain of definition, thereby observing the constraints, and selecting the combination that comes closest to the targeted inductance.

With this approach, invalid parameter combinations as explained in section 3 will inevitably occur. They must either be detected and skipped in the nested loops of the parameter variation step or be detected in the results and discarded afterwards.

The trouble with invalid parameter combinations can be spared by avoiding their occurrence altogether. This can be achieved by varying *dimensionless parameters* within the intervals defined in section 3. To do this, we also need the inverse transformation equations to transform the dimensionless parameters back to dimensional ones after the inductance calculations are done. They are given in ([10], equations (12) – (15)). Note that, for rectangular coils, we adhere to $A \geq B$, so that, in these equations, A must be replaced by B, as was done in equation (5). The inverse equations then read

$$s = \eta B,$$

$$w = \kappa \eta B,$$

with

$$\eta = \frac{\rho}{(N-1)(1+\rho)\kappa + 1},$$

$$h = \frac{s}{\gamma}.$$

The constraints are then considered *after* varying the parameters, by way of selection. The MATLAB code below is based on this procedure. On the PC specified in section 5, it solved the problem within 2.1 seconds.

First, the given data is initialized. A_o and B_o are the outermost coil dimensions, $A_o = A + s$ and $B_o = B + s$, as can be inferred from Fig. 1. We have $A_o = 250$ µm, $B_o = 150$ µm:

```
Ao = 250e-6; Bo = 150e-6; h = 0.9e-6; smin = 1e-6;
Ltarget = 84.0e-9;
```

Next, vectors (`Nv`, `rv`, and `kv`) for the parameters N, ρ, and κ are initialized with sampling values within the intervals defined in section 3 for one of the four ranges of N. Here, the data for the high range ($N = 13 \ldots 20$) is shown.

```
Nv = 13:20;
rv = linspace (0.01, 0.86, 100);
kv = linspace (1.01, 10.0, 30);
Matrix = zeros (length(Nv)*3000, 6);
ind = 0;
```

The inductances of 24000 coils are then calculated by calling the function `L_RectPlanarSpiral` from appendix 4:

```
for i1 = 1 : length(Nv),
   N = Nv(i1);
   for i2 = 1 : length(kv),
      kappa = kv(i2);
      for i3 = 1 : length(rv),
         rho = rv(i3);
         ind = ind + 1;
         eta = rho/((N - 1)*kappa*(1 + rho) + 1);
         so = eta * Bo;
         B = Bo - so;
         A = Ao - so;
         s = eta * B;
         w = kappa * eta *B;
         g = w - s;
         L = L_RectPlanarSpiral (N,A,B,w,s,h);
         Matrix(ind,:) = [N, A, B, s, g, L];
      end
   end
end
```

The `Matrix` now contains the dimensional design parameters and respective inductance of all coil designs. From these, those fulfilling the constraints $s \geq 1$ µm and $g \geq 1$ µm are extracted and stored in `Matrix1`:

```
ind_constraints = Matrix(:,4) >= smin & ...
                  Matrix(:,5) >= smin;
Matrix1 = Matrix(ind_constraints,:);
```

From these, the ones whose calculated inductance does not deviate from the target value by more than 1 % are extracted and stored in `Matrix2`:

```
ind_dev = abs(Matrix1(:,6)-Ltarget)/Ltarget<=0.01;
Matrix2 = Matrix1(ind_dev,:);
```

From these, the ones with the smallest number of windings are selected to keep the resistive loss as small as possible. The resulting designs are stored in `Matrix3`:

```
ind_minN = Matrix2(:,1) == min(Matrix2(:,1));
Matrix3 = Matrix2(ind_minN,:);
```

From the remaining designs, the final solution vector with the smallest deviation of the calculated inductance from the target value is extracted:

```
ind_solution = abs(Matrix3(:,6) - Ltarget) == ...
    min(abs(Matrix3(:,6) - Ltarget));
solution_vector = Matrix3(ind_solution,:)
```

If, in the given range of N, the problem does have a solution, then the solution vector contains all design parameters and the resulting inductance. If there is no solution, the solution vector will be empty, and another one of the four ranges of N defined in section 3 or a new one with $N > 20$ (see section 5) must be tried. For our example problem, the solution is:

$N = 17$, $A = 248.9$ µm, $B = 148.9$ µm, $s = 1.109$ µm, $g = 1.043$ µm, $L = 83.5$ nH.

The calculated DC inductance L is 0.6 % off target. The exact DC inductance calculated with FastHenry2 is 82.5 nH. Thus, the effective error of the inductance formula is 1.2 %, in accordance with the maximum error of 1.8 % as disclosed by linear interpolation of Table 1 for $\Gamma = 1.67$. At 4.0 GHz, the exact inductance decreases by only 0.007 % compared to DC. Hence, at 4.0 GHz, the error of the inductance formula also amounts to 1.2 %. The inductance at 4.0 GHz was computed by requesting 10×10 subfilaments in FastHernry2 to consider the frequency effects, see ([14], section 5). The run time of FastHenry2 on the PC specified in section 5 was 3 hours and 7 minutes.

9. Conclusions

A precise formula for the DC inductance of rectangular planar spiral coils with an aspect ratio of up to 4.0 and having a rectangular conductor cross section with an aspect ratio of height to width not exceeding unity has been derived from physical principles. The formula is scalable; hence, it is valid for coils within any inductance range and of any dimension.

The formula is akin to the current sheet approximation [12], but with the difference that the gaps between the conductor segments are considered. As a consequence, it is much more precise. Its maximum error for the usual range of parameters used for inductors in RFIC's and in antennas in RFID, NFC, and telemetry devices is 2.6 %. This has been tested systematically on almost 194000 reference designs of exactly known inductance. To this end, dimensionless parameters to reduce the number of dimensions of the parameter space by one have been introduced. The formula has also been tested against measurements on 16 RFID antennas manufactured as PCB's. It is based on the method of mean distances [15].

For wireless charging devices and for eddy current sensors for nondestructive testing it has been found that square coils and the formula presented in [14] are to be preferred.

The source code of a MATLAB function for evaluating the formula, together with numerical examples, have been provided. Moreover, an example for solving a coil design problem for RFIC's with constraints as they arise in practical engineering has been presented, together with the complete MATLAB code.

Exact expressions for the GMD, AMSD, and AMD between a rectangle and itself and between two displaced congruent rectangles are derived in the appendices. Those for the AMD and one for the AMSD seem to be new. They have been used to verify known or to derive new approximations, like e.g. for the GMD between two displaced congruent rectangles, equation (20). So far, only an approximation for two displaced line segments was known. One of the exact expressions for the AMSD is used in the inductance formula.

The paper presents the first example in the literature of an application of the method of mean distances where any curtailment in calculating the partial self-inductance of conductor segments as it is often found in the literature (like e.g. neglecting the AMSD and AMD or replacing them by the GMD), leads to a clearly verifiable error in the calculated total inductance. The method of mean distances was originally proposed by Rosa [19], although he did not actually carry it out. To my knowledge, its first full use was reported in [15] where it was also justified mathematically ([15], section 7). But the partial inductance of single wires to which it was applied cannot be measured ([15], section 8). Further, the inductance of the small shorted two-wire transmission lines of a few nH, used as examples of an application to components that are at least measurable in principle, was too small to be measured accurately. Thus, these examples were not suitable either to provide experimental evidence of the usefulness of the method ([15], section 10). The first application to a precisely measurable inductance was reported in [22] on large shorted two-wire transmission lines. But due to the proximity effect occurring in the main conductors, the method of mean distances could only be applied to the small shorting rods, and the effect of neglecting the AMSD and AMD in calculating the inductance of the shorting rods on the total inductance was ≤ 1.5 % ([22], p. 33), comparable to the measurement error of 1 % ([22], p. 32). By contrast, in this paper, neglecting the AMSD and AMD in the calculation of the partial self-inductance of

coils has led to errors in the total inductance of up to 30 %, and up to 16 % for replacing the AMD by the GMD. Due to the scalability of coil inductance ([10], p. 39), these results can be reproduced for coils of any dimension, in any inductance range, and at any frequency low enough to represent DC. Therefore, this paper provides the first experimentally verifiable evidence of the usefulness of the full method of mean distances as introduced in [15].

It has been found that the maximum error of the formula over all parameters except the coil aspect ratio strictly decreases with increasing coil aspect ratio up to a certain limit, depending on the number of turns. Up to this limit, the maximum error for any coil design in function of the coil aspect ratio can be found by linear interpolation of the data provided in this paper. Above this limit, the error has been found to increase or even to become chaotic. Note that the maximum error of the current sheet approximation [12] also decreases, but it is not possible to define a convex domain of definition where the error decreases strictly.

The maximum error of the formula (5.6 %) is clearly larger than the largest contribution (0.4 %) found from the approximations for the mean distances. The conclusion is that the error must originate from the concept of average-sized single-turn coil on which the formula is based. The varying lengths of the parallel conductor segments on one side of the spiral coil are all approximated by the same average length. This has been a prerequisite for using the method of mean distances for a row of rectangles. Thus, considering these length variations in future work may be expected to significantly improve the accuracy of the formula, but at the cost of substantially increasing its complexity, provided that it will still be possible to derive a closed formula at all, rather than just being reverted to the Greenhouse method [9].

Transponder antennas are often manufactured from round wire. It would be desirable to derive a modified formula for coils with circular conductor cross section. Formulae for all respective mean distances can be found in [15], even for the high-frequency limits (but neglecting the proximity effect). The challenge will be that the software FastHenry2 is limited to conductors of rectangular cross section, so that other means for doing exact inductance calculations for the error analysis will have to be sought.

Appendix 1

In this appendix, the exact expression for $\log GMD_2$ is derived, i.e. the logarithm of the GMD between two congruent rectangles of width s and height h, horizontally displaced by the distance w, see Fig. 8, and the exact expression for $\log GMD_1$, the logarithm of the GMD between a single rectangle and itself.

The definition of the GMD is given by the double area integral normalized by $1/A^2$ in equation (7). First, we must find the antiderivative G given by the indefinite integral

$$G(x-x',y-y') = \iint\iint \log\sqrt{(x-x')^2+(y-y')^2}\,dxdx'dydy'. \quad (31)$$

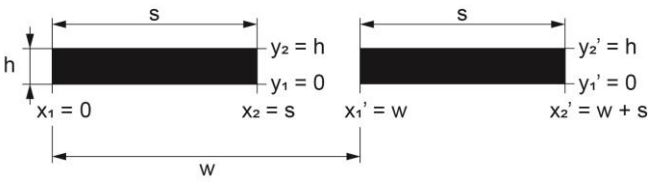

Figure 8: Two horizontally displaced congruent rectangles with the coordinates of the edge points.

Noting that $\log\sqrt{x} = (1/2)\log x$, finding the solution is tedious but straightforward. It was also presented in a different form in [23]. The result is

$$\begin{aligned} G(x-x',y-y') = {} & \\ & -\frac{1}{48}[(x-x')^4 - 6(x-x')^2(y-y')^2 + (y-y')^4] \\ & \qquad \cdot \log[(x-x')^2+(y-y')^2] \\ & +\frac{1}{6}(x-x')(y-y')\left[(x-x')^2 \arctan\frac{y-y'}{x-x'}\right. \\ & \qquad \left. +(y-y')^2 \arctan\frac{x-x'}{y-y'}\right] \\ & -\frac{25}{48}(x-x')^2(y-y')^2. \end{aligned} \quad (32)$$

Apart from the normalizing factor $1/A^2$ in equation (7), we need the definite integral

$$I_G = \int_{y_1'}^{y_2'}\int_{y_1}^{y_2}\int_{x_1'}^{x_2'}\int_{x_1}^{x_2} \log\sqrt{(x-x')^2+(y-y')^2}\,dxdx'dydy'. \quad (33)$$

The coordinates of the edge points in Fig. 8 also represent the integration limits. According to Fig. 8, they are

$$x_1 = 0,\ x_2 = s,\ y_1 = 0,\ y_2 = h, \quad (34a)$$
$$x_1' = w,\ x_2' = w+s,\ y_1' = 0,\ y_2' = h. \quad (34b)$$

With the limits (34a) and (34b), the integral I_G reads

$$\begin{aligned} I_G = {} & 4G(-w,0) \\ & -2G(-w,h) - 2G(-w,-h) \\ & -2G(s-w,0) - 2G(-w-s,0) \\ & +G(s-w,h) + G(s-w,-h) \\ & +G(-w-s,h) + G(-w-s,-h). \end{aligned} \quad (35)$$

According to equation (32), the antiderivative G is an even function of the differences $x-x'$ and $y-y'$. Therefore, the signs of the differences in the arguments of G don't matter, and equation (35) simplifies to

$$\begin{aligned} I_G = {} & -4G(w,h) + 4G(w,0) \\ & +2G(w-s,h) - 2G(w-s,0) \\ & +2G(w+s,h) - 2G(w+s,0). \end{aligned} \quad (36)$$

We must normalize the integral (36) by the square of the rectangular area $A = sh$, which was omitted in equation (33):

$$\log GMD_2 = \frac{1}{(sh)^2} I_G \,. \tag{37}$$

Evaluating the six terms of equation (36) with the help of the antiderivative (32), equation (37) yields

$$\begin{aligned}
\log GMD_2 = \frac{1}{(sh)^2}\Bigg\{ & \frac{1}{6} w^4 \log\sqrt{1+\frac{h^2}{w^2}} \\
& + \frac{1}{12}(-6w^2h^2 + h^4)\cdot\log(w^2+h^2) \\
& - \frac{1}{12}(w+s)^4 \log\sqrt{1+\frac{h^2}{(w+s)^2}} \\
& - \frac{1}{24}[-6(w+s)^2h^2 + h^4]\cdot\log[(w+s)^2+h^2] \\
& - \frac{1}{12}(w-s)^4 \log\sqrt{1+\frac{h^2}{(w-s)^2}} \\
& - \frac{1}{24}[-6(w-s)^2h^2 + h^4]\cdot\log[(w-s)^2+h^2] \\
& - \frac{2}{3}wh\left(w^2\arctan\frac{h}{w} + h^2\arctan\frac{w}{h}\right) \\
& + \frac{1}{3}(w+s)h\left[(w+s)^2\arctan\frac{h}{w+s} + h^2\arctan\frac{w+s}{h}\right] \\
& + \frac{1}{3}(w-s)h\left[(w-s)^2\arctan\frac{h}{w-s} + h^2\arctan\frac{w-s}{h}\right]\Bigg\} \\
& - \frac{25}{12}\,.
\end{aligned} \tag{38}$$

It is possible to rewrite equation (38) in a simpler and more symmetrical form. But then it loses its numerical stability for large w and $\gamma = 1$ for the two higher ranges of N. This stability is important in subsection 4.3. Therefore, the equation is presented in the form (38)[3].

An equivalent expression was also given by Gray ([24], equation (113)) and revised by Rosa ([25], equation (8)), but as a function of the gap g instead of the winding distance w, and for the more general case of the GMD between two differently sized rectangles. The symmetrical form of equation (38) can also be derived from Higgins' formulae ([26], equations (21) – (24)), which give the logarithm of the GMD between two arbitrarily positioned rectangles. All three results, i.e. equation (38), ([25], equation (8)), and ([26], equations (21) – (24)), are analytically equivalent.

In the limit of vanishing displacement $w \to 0$, equation (38) turns into the exact expression for $\log GMD_1$, the GMD between a single rectangle (of width s and height h) and itself as published by Maxwell ([27], § 692 (6)) and Gray ([24], equation (114)):

$$\begin{aligned}
\log GMD_1 = {} & \log\sqrt{s^2+h^2} - \frac{1}{6}\frac{s^2}{h^2}\log\sqrt{1+\frac{h^2}{s^2}} \\
& - \frac{1}{6}\frac{h^2}{s^2}\log\sqrt{1+\frac{s^2}{h^2}} \\
& + \frac{2}{3}\left(\frac{s}{h}\arctan\frac{h}{s} + \frac{h}{s}\arctan\frac{s}{h}\right) - \frac{25}{12}\,.
\end{aligned} \tag{39}$$

Appendix 2

In this appendix, the exact expression for $AMSD_2{}^2$ between two rectangles as shown in Fig. 8 and the exact expression for $AMSD_1{}^2$ between a rectangle and itself are derived. The definition of the AMSD squared is given by the double area integral normalized by $1/A^2$ in equation (13).

Equations (31) and (33) apply analogously, only that the logarithm and the square root in the integrand are omitted, while the definite integral in the limits (34) is designated by I_S and the antiderivative by S, which reads

$$S(x-x', y-y') = \int\int\int\int [(x-x')^2 + (y-y')^2]\, dx dx' dy dy'.$$

The solution is easily found to be

$$S(x-x', y-y') = \frac{1}{24}(x-x')^2(y-y')^2[(x-x')^2 + (y-y')^2]. \tag{40}$$

Equations (36) and (37) apply analogously, apart from the fact that, from equation (40), it is evident that S vanishes when $x - x'$ or $y - y'$ is naught. Hence, the analog to equation (36) shortens to

$$I_S = -4S(w,h) + 2S(w-s,h) + 2S(w+s,h). \tag{41}$$

Evaluating the three terms of equation (41) with the help of the antiderivative (40) and the normalization (37) results in

$$AMSD_2{}^2 = w^2 + \frac{1}{6}(s^2+h^2). \tag{42}$$

For $w = 0$ one obtains the AMSD squared between a single rectangle and itself:

$$AMSD_1{}^2 = \frac{1}{6}(s^2+h^2). \tag{43}$$

Equation (43) was also presented in ([13], equation (3.25)) without derivation. The result (42), though, could not be found in the literature. It was checked with the help of numerical integration of the normalized double area integrand in equation (13) by iterating the MATLAB function

[3] Note that equation (38) is suitable for calculating $\log GMD_{L,2}$ but *not* $\log GMD_{\bar{c}}$, since for large w and small h, equation (38) becomes numerically unstable unless $s = h$, see subsection 4.3.

`integral2`. The equality could be established to a relative accuracy of 10^{-10}.

Appendix 3

In this appendix, the exact expression for AMD_2 between two rectangles as shown in Fig. 8 and the exact expression for AMD_1 between a rectangle and itself are derived. The definition of the AMD is given by the double area integral normalized by $1/A^2$ in equation (15).
Equations (31) and (33) apply analogously, only that the logarithm in the integrand is omitted, while the definite integral in the limits (34) is designated by I_{Ar} and the antiderivative by Ar. It is given by

$$Ar(x-x',y-y') = \int\int\int\int \sqrt{(x-x')^2+(y-y')^2}\,dx\,dx'\,dy\,dy'.$$

Finding the solution is tedious but straightforward. It reads

$$\begin{aligned} &Ar(x-x',y-y') = \\ &= -\frac{1}{60}[(x-x')^4 - 3(x-x')^2(y-y')^2 + (y-y')^4] \\ &\qquad \cdot\sqrt{(x-x')^2+(y-y')^2} \\ &\qquad +\frac{1}{24}(x-x')(y-y') \\ &\cdot\left\{(y-y')^3\log\left[x-x'+\sqrt{(x-x')^2+(y-y')^2}\right]\right. \\ &\left.+(x-x')^3\log\left[y-y'+\sqrt{(x-x')^2+(y-y')^2}\right]\right\}. \end{aligned} \quad (44)$$

According to equation (44), only the first summand of the antiderivative Ar is an even function of the differences $x-x'$ and $y-y'$. Its second summand is an odd function. Thus, the antiderivative does not possess any simplifying symmetries. Therefore, the expression for the definite integral cannot be simplified. It remains in the form analogous to equation (35):

$$\begin{aligned} I_{Ar} = {} & 4Ar(-w,0) \\ & -2Ar(-w,h) - 2Ar(-w,-h) \\ & -2Ar(s-w,0) - 2Ar(-w-s,0) \\ & +Ar(s-w,h) + Ar(s-w,-h) \\ & +Ar(-w-s,h) + Ar(-w-s,-h). \end{aligned} \quad (45)$$

Evaluating equation (45) with the help of the antiderivative (44) and considering the normalization (37) yields equation (46)[4].
The limit $w \to 0$ of equation (46) does not exist. The AMD between a single rectangle and itself must be calculated separately. It can be deduced from equation (45) by setting $w = 0$ with $A_r(0,0) = 0$. In the antiderivative (44), the second summand is an odd function that vanishes when $x-x'$ or $y-y'$ is naught, so that only the first summand remains, which is even, hence $A_r(s,0) = A_r(-s,0)$ and $A_r(0,h) = A_r(0,-h)$.

$$\begin{aligned} AMD_2 = {} & \frac{1}{s^2}\left(\frac{1}{15}\left[\frac{w^4}{h^2} - 3w^2 + h^2\right]\sqrt{w^2+h^2}\right. \\ & +\frac{1}{6}wh^2\log\left[-w+\sqrt{w^2+h^2}\right] \\ & \left.+\frac{1}{12}\frac{w^4}{h}\log\left[\frac{-h+\sqrt{w^2+h^2}}{h+\sqrt{w^2+h^2}}\right]\right) \\ & -\frac{1}{30}\left\{\left[\frac{(w-s)^4}{h^2} - 3(w-s)^2 + h^2\right]\sqrt{(w-s)^2+h^2}\right. \\ & \left.+\left[\frac{(w+s)^4}{h^2} - 3(w+s)^2 + h^2\right]\sqrt{(w+s)^2+h^2}\right\} \\ & -\frac{1}{12}h^2\left\{(w-s)\log\left[-(w-s)+\sqrt{(w-s)^2+h^2}\right]\right. \\ & \left.+(w+s)\log\left[-(w+s)+\sqrt{(w+s)^2+h^2}\right]\right\} \\ & +\frac{1}{24}\frac{1}{h}\left\{(w-s)^4\log\frac{h+\sqrt{(w-s)^2+h^2}}{-h+\sqrt{(w-s)^2+h^2}}\right. \\ & \left.\left.+(w+s)^4\log\frac{h+\sqrt{(w+s)^2+h^2}}{-h+\sqrt{(w+s)^2+h^2}}\right\}\right) \\ & +\frac{1}{3}\frac{1}{h^2}(2w^3+ws^2). \end{aligned} \quad (46)$$

The definite integral (45) then simplifies to

$$\begin{aligned} I_{Ar} = {} & -4Ar(0,h) - 4Ar(s,0) \\ & +Ar(s,h) + Ar(s,-h) \\ & +Ar(-s,h) + Ar(-s,-h). \end{aligned} \quad (47)$$

Evaluating equation (47) with the help of the antiderivative (44) and considering the normalization (37) yields

$$\begin{aligned} AMD_1 = {} & \frac{1}{15}\left[\frac{s^3}{h^2} + \frac{h^3}{s^2} - \left(\frac{s^2}{h^2} + \frac{h^2}{s^2} - 3\right)\sqrt{s^2+h^2}\right] \\ & +\frac{1}{6}\left(\frac{h^2}{s}\log\frac{s+\sqrt{s^2+h^2}}{h} + \frac{s^2}{h}\log\frac{h+\sqrt{s^2+h^2}}{s}\right). \end{aligned} \quad (48)$$

Equation (48) is symmetrical on exchanging s and h, as are equations (39) and (43), as they all must be. The results (44), (46), and (48) could not be found in the literature. They were checked with the help of numerical integration of the normalized double area integrand in equation (15) by iterating the MATLAB function `integral2`. The equality could be established to a relative accuracy of 10^{-10}.

[4] Note that equation (46) is suitable for calculating AMD_L but *not* $AMD_{\tilde{c}}$, since for large w and small h, equation (46) becomes numerically unstable, see subsection 4.3.

Appendix 4

Source code of the MATLAB function `L_RectPlanarSpiral`:

```
function [L, rho] = L_RectPlanarSpiral ...
                    (N, A, B, w, s, h)
if B > A,
   Asave = A;
   A = B;
   B = Asave;
end
L = NaN;
mu0 = 4 * pi * 1e-7;
mu4pi = mu0 / (4*pi);
mess = 'Invalid parameter combination.';
a = A - (N - 1)*w;
b = B - (N - 1)*w;
rho = ((N - 1)*w + s) / (B - (N - 1)*w);
switch N,
 case 2;
  if rho > 0.36001, disp(mess); return; end
 case {3, 4, 5, 6, 7};
  if rho > 0.52001, disp(mess); return; end
 case {8, 9, 10, 11, 12};
  if rho > 0.78001, disp(mess); return; end
 case {13, 14, 15, 16, 17, 18, 19, 20};
  if rho > 0.86001, disp(mess); return; end
end
if N >= 21;
  if rho>(N-1)/(N+1), disp(mess); return; end
end
k = 1 : N - 1;
ks = -(N - 1) :  N - 1;
log_GMD1 = log(s + h) - 3/2;
log_GMD2 = @(w) log(s + h) + log(w/(2*s)) -...
             (-1.46*s/h + 1.45)/(2.14*s/h + 1);
GMD1 = 0.2235*(s + h);
GMD2 = @(w) exp(log_GMD2(w));
AMD1 = GMD1;
AMD2 = @(w) GMD2(w);
AMSD1sq = 1/6*(s^2 + h^2);
AMSD2sq = @(w) w.^2;
log_GMD_L = (N*(log_GMD1) + ...
           2*sum((N-k).*log_GMD2(k*w))) / N^2;
AMSD_L = (N*AMSD1sq + ...
           2*sum((N-k).*AMSD2sq(k*w))) / N^2;
AMD_L = (N*AMD1 + ...
              2*sum((N-k).*AMD2(k*w))) / N^2;
log_GMD_a = sum((N-abs(ks)).* ...
                          log(a + ks*w)) / N^2;
log_GMD_b = sum((N-abs(ks)).* ...
                          log(b + ks*w)) / N^2;
AMSD_a = sum((N-abs(ks)).* ...
                       AMSD2sq(a + ks*w)) / N^2;
AMSD_b = sum((N-abs(ks)).* ...
                       AMSD2sq(b + ks*w)) / N^2;
AMD_a = sum((N-abs(ks)).*(a + ks*w)) / N^2;
AMD_b = sum((N-abs(ks)).*(b + ks*w)) / N^2;

La = mu4pi * 2 * (a*log(a+sqrt(a^2+AMSD_L))...
  - a*log_GMD_L - sqrt(a^2 + AMSD_L) + AMD_L);
Lb = mu4pi * 2 * (b*log(b+sqrt(b^2+AMSD_L))...
  - b*log_GMD_L - sqrt(b^2 + AMSD_L) + AMD_L);
Ma = mu4pi * 2 * (a*log(a+sqrt(a^2+AMSD_b))...
  - a*log_GMD_b - sqrt(a^2 + AMSD_b) + AMD_b);
Mb = mu4pi * 2 * (b*log(b+sqrt(b^2+AMSD_a))...
  - b*log_GMD_a - sqrt(b^2 + AMSD_a) + AMD_a);
L = 2 * N^2 * (La + Lb - (Ma + Mb));
```


Acknowledgements

The author wishes to thank LEGIC Identsystems AG for granting the time to work on this project.

References

[1] J. Chen and J. J. Liou, On-Chip Spiral Inductors for RF Applications: An Overview, *Journal of Semiconductor Technology and Science*, vol. 4, no. 3, 149-167, 2004.

[2] D. Paret, *RFID and Contactless Smart Card Applications,* John Wiley & Sons, Ltd, West Sussex, 2005.

[3] D. Paret, *Antenna Designs for NFC Devices*, ISTE Ltd, London, 2016.

[4] R. A. Potyrailo, C. Surman, S. Go, Y. Lee, T. Sivavec, and W. G. Morris, Development of radio-frequency identification sensors based on organic electronic sensing materials for selective detection of toxic vapors, *Journal of Applied Physics*, vol. 106, 124902-1 - 124902-6, 2009.

[5] J. M. Park, K. B. Lee, and K. H. Baek, Apparatus and Method for Wireless Charging, *United States Patent* US 9,590,446 B2, 2017.

[6] C. Panchal, S. Stegen, an J. Lu, Review of static and dynamic wireless electric vehicle charging system, *Engineering Science and Technology, an International Journal*, vol. 21, no. 5, 922-937, 2018.

[7] T. P. Theodoulidis and E. E. Kriezis, Impedance evaluation of rectangular coils for eddy current testing of planar media, *Ndt & E International*, vol. 35, no. 6, 407-414, 2002.

[8] R. J. Ditchburn and S. K. Burke, Planar rectangular spiral coils in eddy-current non-destructive inspection, *Ndt & E International*, vol. 38, no. 8, 690-700, 2005.

[9] H. M. Greenhouse, Design of Planar Rectangular Microelectronic Inductors, *IEEE Trans. on Parts, Hybrids, and Packaging*, vol. 10, no. 2, 101-109, 1974.

[10] H. A. Aebischer, Comparative Study of Analytical Inductance Formulae for Square Planar Spiral Inductors, *Advanced Electromagnetics*, vol. 7, no. 5, 3-48, 2018. DOI: https://dx.doi.org/10.7716/aem.v7i5.862

[11] J. Crols, P. Kinget, J. Craninckx, and M. Steyaert, An Analytical Model of Planar Inductors on Lowly Doped Silicon Substrates for High Frequency Analog Design up to 3 GHz, *IEEE Symposium on VLSI Circuits*, *Honolulu, Digest of Technical Papers*, 28-29, 1996.

[12] S. S. Jayaraman, V. Vanukuru, D. Nair, and A. Chakravorty, A Scalable, Broadband, and Physics-Based Model for On-Chip Rectangular Spiral Inductors, *IEEE Trans. on Magnetics*, vol. 55, no. 9, 8402006, 2019.

[13] S. S. Mohan, *The design, modeling and optimization of on-chip inductor and transformer circuits*, Ph.D. dissertation, Dept. Elect. Eng. Stanford University, CA, USA, 2000. http://cc.ee.nchu.edu.tw/~aiclab/public_htm/VCO/Theses/1999mohan.pdf

[14] H. A. Aebischer, Inductance Formula for Square Planar Spiral Inductors with Rectangular Conductor Cross

Section, *Advanced Electromagnetics*, vol. 8, no. 4, 80-88, 2019. DOI: https://dx.doi.org/10.7716/aem.v8i4.1074

[15] H. A. Aebischer and B. Aebischer, Improved Formulae for the Inductance of Straight Wires, *Advanced Electromagnetics*, vol. 3, no. 1, 31-43, 2014. DOI: https://dx.doi.org/10.7716/aem.v3i1.254

[16] M. Kamon, M. J. Tsuk, and J. K. White, FASTHENRY: A Multipole-Accelerated 3-D Inductance Extraction Program, *IEEE Trans. on Microwave Theory and Techniques*, vol. 42, no. 9, 1750-1758, 1994.

[17] W. M. Haynes, Th. J. Bruno, and D. R. Lide, *CRC Handbook of Chemistry and Physics*, 95th ed., Internet Version 2015, p. 12-41, 2015.

[18] C. R. Paul, *Inductance*, John Wiley & Sons, Hoboken NJ, 2010.

[19] E. B. Rosa, The Self and Mutual Inductances of Linear Conductors, *Bulletin of the Bureau of Standards*, vol. 4, no. 2, 301-344, Washington, 1908.

[20] F. W. Grover, *Inductance Calculations: Working Formulas and Tables*, Dover Publications, New York, 2004, first published by D. Van Nostrand Co., New York, 1946.

[21] E. B. Rosa, Calculation of the Self-Inductance of Single-Layer Coils, *Bulletin of the Bureau of Standards*, vol. 2, no. 2, 161-187, Washington, 1906.

[22] H. A. Aebischer and H. Friedli, Analytical Approximation for the Inductance of Circularly Cylindrical Two-Wire Transmission Lines with Proximity Effect, *Advanced Electromagnetics*, vol. 7, no. 1, 25-34, 2018, DOI: http://dx.doi.org/10.7716/aem.v7i1.516

[23] W. T. Weeks, L. L. Wu, M. F. McAllister, and A. Singh, Resistive and Inductive Skin Effect in Rectangular Conductors, *IBM J. Res. Develop.*, vol. 23, no. 6, 652-660, 1979.

[24] A. Gray, *The theory and practice of absolute measurements in electricity and magnetism*, MacMillan & Co., London and New York, vol. II, part I, 1893.

[25] E. B. Rosa, On the Geometrical and Mean Distances of Rectangular Areas and the Calculation of Self-Inductance, *Bulletin of the Bureau of Standards*, vol. 3, no. 1, 1-41, Washington, 1907.

[26] T. J. Higgins, Formulas for the Geometric Mean Distances of Rectangular Areas and of Line Segments, *Journal of Applied Physics*, vol. 14, 188-195, 1943.

[27] J. C. Maxwell, *A Treatise on Electricity and Magnetism*, vol. 2., Dover Publications, New York, 1954, unabridged 3rd ed. of 1891.